JOURNAL OF AGRICULTURAL AND FOOD CHEMISTRY

pubs.acs.org/JAFC

Article

One-Pot Biosynthesis of 2-Keto-4-hydroxybutyrate from Cheap C1 Compounds Using Rationally Designed Pyruvate Aldolase and Methanol Dehydrogenase

Yeon-Ju Jeong,[‖] Pil-Won Seo,[‖] Min-Ju Seo,[‖] Su-Bin Ju, Jeong-Sun Kim,* and Soo-Jin Yeom*

Cite This: *J. Agric. Food Chem.* 2023, 71, 4328−4336

Read Online

ACCESS | Metrics & More | Article Recommendations | Supporting Information

ABSTRACT: One-carbon chemicals (C 1s) are potential building blocks as they are cheap, sustainable, and abiotic components. Methanol-derived formaldehyde can be another versatile building block for the production of 2-keto-4-hydroxyacid derivatives that can be used for amino acids, hydroxy carboxylic acids, and chiral aldehydes. To produce 2-keto-4-hydroxybutyrate from C 1s in an environment-friendly way, we characterized an aldolase from *Pseudomonas aeruginosa* PAO1 (*Pa*ADL), which showed much higher catalytic activity in condensing formaldehyde and pyruvate than the reported aldolases. By applying a structure-based rational approach, we found a variant (*Pa*ADL$^{V121A/L241A}$) that exhibited better catalytic activities than the wild-type enzyme. Next, we constructed a one-pot cascade biocatalyst system by combining *Pa*ADL and a methanol dehydrogenase (MDH) and, for the first time, effectively produced 2-keto-4-hydroxybutyrate as the main product from pyruvate and methanol via an enzymatic reaction. This simple process applied here will help design a green process for the production of 2-keto-4-hydroxyacid derivatives.

KEYWORDS: *formaldehyde, pyruvate, methanol, pyruvate aldolase, Pseudomonas aeruginosa PAO1, 2-keto-4-hydroxybutyrate*

INTRODUCTION

One-carbon chemicals (C 1s) are potential feedstocks that have recently gained attention and preference in the industrial field due to their natural abundance, low production cost, and availability as industrial byproducts.[1,2] However, native pathways to utilize these chemicals are scarce in most biotechnologically relevant microorganisms. Recent advances in synthetic biology, genome engineering, and laboratory evolution are enabling the first steps toward the creation of synthetic C1-utilizing microorganisms.[3−5] For this, there is a high need for a new synthetic C1-utilizing enzymes that form carbon−carbon (C−C) bonds between chemicals including C 1s.[1]

Among C 1s, formaldehyde is an emerging C1 substrate since it can be diversely prepared from carbon monoxide (CO), carbon dioxide (CO_2), formic acid (HCOOH), methane (CH_4), and especially methanol (CH_3OH) by biological or chemical means.[6,7] Especially, methanol is interesting because it is produced also from biomass-derived synthesis gas and reduction of CO_2 and is generally available at a cheaper price than sugar.[8−10] Oxidation of methanol to formaldehyde by methanol dehydrogenase (MDH), one of the key steps in methanol utilization, is the initial and rate-limiting step in methanol bioconversion because of its low catalytic activity and substrate affinity.[11,12] MDH is also thermodynamically unstable. In the previous study, we successfully engineered the methanol dehydrogenase from *Lysinibacillus xylanilyticus* (*Lx*MDH) to possess much higher catalytic efficiency than the wild-type enzyme.[13,14] Conversion of formaldehyde into value-added molecules is substantially challenging because of its toxicity and symmetrical reactivity. Therefore, aldolases are very attractive since they stereospecifically and efficiently catalyze the chemical reaction on a C−C bond between ketones and aldehydes,[15] which is poor in chemical aldol reactions.[16]

Pyruvate aldolase reversibly mediates the C−C bond formation between pyruvate and aldehydes to produce 4-hydroxy-2-ketoacids that are less exploited in organic synthesis.[17−20] Pyruvate aldolase is a potential biocatalyst for condensing formaldehyde and pyruvate to produce 2-keto-4-hydroxybutyrate, a valuable building block for the synthesis of L-homoserine, 3-hydroxypropionic acid, and 1,3-propanediol, which are important starting materials in the manufacture of biocompatible plastic and polytrimethylene terephthalate.[19,21−31] In this regard, the high production of 2-keto-4-hydroxybutyrate from cheap materials is of great interest. Recently, 2-keto-4-hydroxybutyrate as an intermediate in metabolic pathways has been produced by several enzymes, such as 2-keto-3-deoxy-L-rhamnonate aldolase from *Escherichia coli* (*Ec*YfaU), 2-keto-4-hydroxybutyrate aldolase from *E. coli* K-12 (*Ec*KHB), and 2-keto-4-hydroxyglutarate aldolase from *Rattus norvegicus* (*Rn*KHG), *Homo sapiens* (*Hs*KHG), and *Bos taurus* (*Bt*KHG).[28] Among them, *Ec*YfaU is unique in that it was rationally engineered for nucleophile selectivity and stereoselectivity[19] and used for the production of amino acids via a multienzyme cascade reaction.[21] *Ec*YfaU was also

Received: December 28, 2022
Revised: February 20, 2023
Accepted: February 22, 2023
Published: March 1, 2023

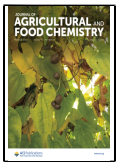

https://doi.org/10.1021/acs.jafc.2c09108
J. Agric. Food Chem. 2023, 71, 4328−4336

Scheme 1. Scheme of 2-Keto-4-hydroxybutyrate Production from Methanol-Derived Formaldehyde and Pyruvate Using Methanol Dehydrogenase from *Lysinibacillus xylanilyticus* (*Lx*MDH) and Pyruvate Aldolase from *Pseudomonas aeruginosa*PAO1 (*Pa*ADL)

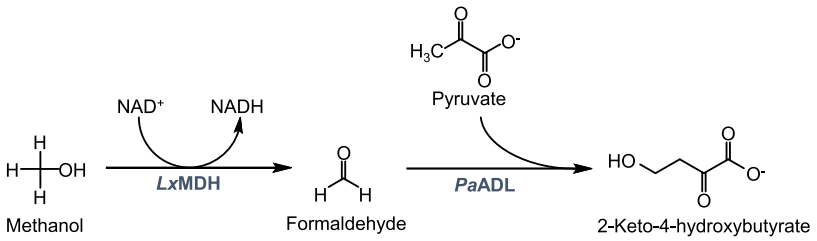

used to direct formaldehyde into 2-keto-4-hydroxybutyrate for the biosynthesis of 1,3-propanediol in *E. coli*.[28] However, *Ec*YfaU may have limitations for industrial applications because the enzyme is susceptible to inhibition by its substrate, namely, formaldehyde or pyruvate.[32] To overcome this limitation, the development of a new pyruvate aldolase with high catalytic activity and enhanced substrate tolerance is suggested.

Here, we report a pyruvate aldolase from *Pseudomonas aeruginosa* PAO1 (*Pa*ADL) that has a much higher catalytic activity and is more tolerant to substrates than *Ec*YfaU. Its crystal structure was determined, and the structure-based rational design of *Pa*ADL generated a gallery of variants that showed higher activities than the wild-type enzyme. Furthermore, we designed and established a one-pot cascade reaction in an eco-friendly biosynthetic way to produce 2-keto-4-hydroxybutyrate (C4) from methanol (C1) by mixing *Pa*ADL with *Lx*MDH (Scheme 1).

MATERIALS AND METHODS

Gene Cloning and Site-Directed Mutagenesis of Aldolase. The *Ec*YfaU (GenBank accession no. APQ20856.1) and *Pa*ADL genes (GenBank accession no. AAC75305) were synthesized for expression in *E. coli* by Cosmo Genetech (Seoul, Republic of Korea) and amplified using polymerase chain reaction (PCR) with primers (listed in Table S1) designed for ligation-independent cloning (LIC).[33] The PCR product was treated with T4 DNA polymerase (New England Biolabs, Hertfordshire, U.K.) and ligated with T4 DNA polymerase-treated pLIC.B4 vector (Table S1).[34] The target gene was designed to translate the protein in a fused state with a His_6, maltose-binding protein (MBP), and tobacco etch virus (TEV) protease cleavage site at the N-terminus of the protein. Site-directed mutagenesis of *Pa*ADL was performed using the overlap PCR method[35] on pLIC.B4-*Pa*ADL (Table S1). The phylogenic tree was constructed using the unweighted pair group method with arithmetic mean (UPGMA) algorithm using the MEGA X (molecular evolutionary genetic analysis) program based on the *p*-distance value. Sequence alignment was performed based on the amino acid sequences from the NCBI database using Clustal W.[36]

Enzyme Expression and Purification of Aldolase. After transformation of the constructed recombinant plasmid into *E. coli* BL21 (DE3) Star (Table S1), cells were grown in Luria−Bertani media containing 50 μg mL^{-1} of ampicillin at 37 °C. When OD_{600} reached 0.5, the expression of the fusion protein was induced by adding 0.1 mM of isopropyl β-D-thiogalactopyranoside, and then the cultured cells were incubated with shaking at 150 rpm at 18 °C for 16 h. The culture was harvested by centrifugation at 8660*g* at 4 °C. The cell pellet was resuspended in an ice-cold lysis buffer containing 20 mM Tris-HCl (pH 7.5), 500 mM NaCl, and 1 mM β-mercaptoethanol (β-ME) with 10 mM phenylmethylsulfonyl fluoride and disrupted by sonication. The supernatant was collected by centrifugation at 31,660*g* for 30 min at 4 °C and loaded onto a Ni-charged immobilized metal ion affinity chromatography column (ELPIS, Daejeon, Republic of Korea). The bound proteins were eluted by a step gradient of imidazole in the lysis buffer. For the crystallization of *Pa*ADL, the recombinant protein was digested with the TEV protease to remove the His_6-MBP tag and dialyzed against in a buffer containing 20 mM Tris-HCl at pH 7.5 and 1 mM β-ME. *Pa*ADL was further isolated using a HiTrap Q column (GE Healthcare, Uppsala, Sweden), which was operated with a linear NaCl gradient (0−1.0 M).

Crystallization and Structure Determination. For crystallization, the purified *Pa*ADL was concentrated to 31 mg mL^{-1} in 20 mM tris−HCl (pH 7.5) and 200 mM NaCl. Protein concentration was determined by considering the extinction coefficient of 0.906 mg mL^{-1} cm^{-1} at 280 nm, which was calculated from the amino acid sequence. The crystals suitable for diffraction experiments were obtained in 200 mM sodium iodide and 24% (w/v) poly(ethylene glycol) (PEG) 3350 using the hanging-drop vapor-diffusion method. For diffraction experiments, the crystals were immersed into the precipitant solution containing an additional 10% (v/v) glycerol as a cryoprotectant for 5 s and placed in the 100 K nitrogen-gas stream. Diffraction data of *Pa*ADL was collected using the beamline BL-11C of the Pohang Accelerator Laboratory (PAL, Pohang, Republic of Korea). The indexing, integration, and scaling of reflections were conducted using the HKL2000 suite.[37] The electron-density map of *Pa*ADL was calculated by the molecular replacement method using the PHENIX program[38] with *Ec*YfaU (PDB ID 2VWT) as the search model. Further model building was done manually using WinCoot,[39] and subsequent refinement was performed using PHENIX.[38] The data collection and refinement statistics are summarized in Table S2. The atomic coordinates and structure factors were deposited in the Protein Data Bank (www.rcsb.org/pdb) with accession ID 7V8T.

Characterization of Aldolase Based on Temperature, pH, and Metal Ions. The effect of temperature on enzyme activity was monitored as a function of time by applying the enzyme solution at different temperatures (20, 25, 30, 35, 40, 45, 50, and 55 °C) in 50 mM of piperazine-*N*,*N*′-bis(2-ethanesulfonic acid) (PIPES, pH 7.0) buffer containing 0.05 mg mL^{-1} of enzyme, 1 mM of Mg^{2+} with 100 mM of formaldehyde and 100 mM of pyruvate for 10 min. To evaluate the effect of pH on aldolase activity, pH values were varied from 6.5 to 9.5 in the buffers of 50 mM PIPES (pH 6.5−7.5), 50 mM *N*-(2-hydroxyethyl)piperazine-*N*′-(3-propanesulfonic acid) (EPPS, pH 7.5−8.5), and 50 mM *N*-cyclohexyl-2-aminoethanesulfonic acid (CHES, pH 8.5−9.5), which contain 1 mM Mg^{2+} with 100 mM formaldehyde and 100 mM pyruvate for 10 min at 45 °C. To investigate the effect of metal ions on enzyme activity, an enzyme assay was carried out after treatment with 1 mM ethylenediaminetetraacetic acid (EDTA) at 4 °C for 2 h or after the addition of 1 mM of each metal ion, such as Mg^{2+}, Mn^{2+}, Co^{2+}, Zn^{2+}, Ni^{2+}, Cu^{2+}, or Ca^{2+}. The reactions were performed in 50 mM CHES buffer (pH 9.0) containing each metal ion with 100 mM formaldehyde and 100 mM pyruvate for 10 min at 45 °C.

Activity Assay of *Pa*ADL Variants. The aldol reactions of *Pa*ADL variants were performed in 50 mM CHES buffer (pH 9.0) containing 0.05 mg mL^{-1} of enzyme, 1 mM of Mg^{2+}, 5 mM of formaldehyde, and 5 mM of pyruvate for 10 min at 45 °C. One unit (U) of enzyme activity was defined as the amount of enzyme required to produce 1 μmol of 2-keto-4-hydroxybutyrate per min. The specific

https://doi.org/10.1021/acs.jafc.2c09108
J. Agric. Food Chem. 2023, 71, 4328−4336

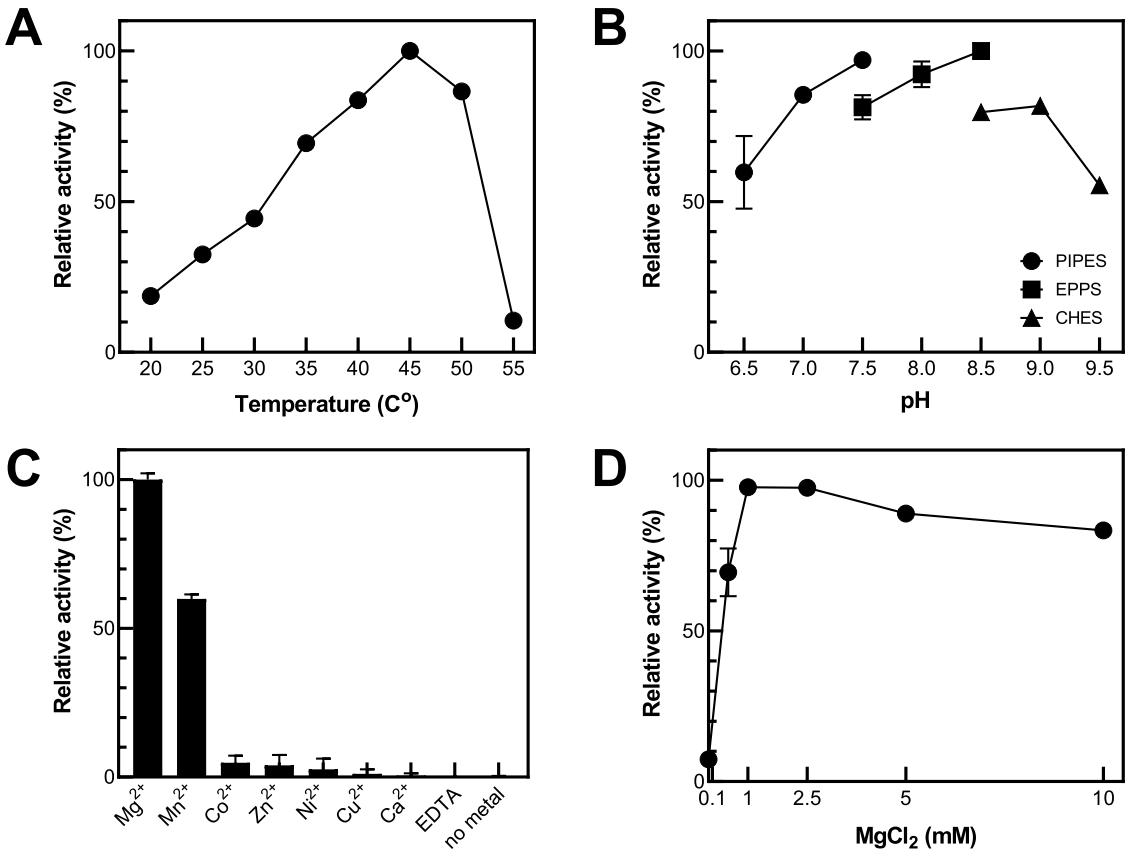

Figure 1. Effects of temperature, pH, and metal ions on *Pa*ADL activity. (A) Temperature: the reactions were performed in 50 mM PIPES buffer (pH 7.0) containing 1 mM Mg^{2+} and 0.05 mg mL^{-1} of enzyme for 10 min. (B) pH: the reactions were performed in 50 mM PIPES, 50 mM EPPS, or 50 mM CHES buffer containing 1 mM of Mg^{2+} and 0.05 mg mL^{-1} of enzyme at 45 °C for 10 min. (C) Metal ions: the reactions were performed in 50 mM CHES buffer (pH 9.0) containing 1 mM of each metal ion and 0.05 mg mL^{-1} of enzyme at 45 °C for 10 min. (D) Concentration of Mg^{2+}: the reactions were performed in 50 mM CHES buffer (pH 9.0) containing 0−10 mM of Mg^{2+} and 0.05 mg mL^{-1} of enzyme at 45 °C for 10 min. All experiments were performed at least twice, and *Pa*ADL activity was determined using HPLC.

activities of these enzymes were defined as the produced amount of product per unit reaction time per enzyme amount.

Kinetic Parameter. The apparent kinetic parameters of *Pa*ADL^{WT}, *Pa*ADL^{V121A}, *Pa*ADL^{L241A}, or *Pa*ADL$^{V121A/L241A}$ for formaldehyde (5−150 mM) and pyruvate (5−150 mM) were determined in a steady-state assumption of 10 min reactions in 50 mM CHES buffer (pH 9.0) containing each 0.005 mg mL^{-1} of enzyme and 1 mM of Mg^{2+} at 45 °C. For the kinetics, the other substrate concentration was fixed at 100 mM because the other substrate concentration had no influence on the reaction. The k_{cat} and K_m values were determined by nonlinear regression with the Michaelis−Menten equation using the GraphPad Prism 6 software (GraphPad Software, San Diego, CA).

Optimization of Reaction Conditions for 2-Keto-4-hydroxybutyrate Production. Unless otherwise stated, the reaction was performed in 50 mM CHES buffer (pH 9.0) with 1 mM Mg^{2+} at 45 °C for 2 h. To determine the optimal concentration of *Pa*ADL^{WT}, 0.01−0.5 mg mL^{-1} of enzyme was incubated with 100 mM of formaldehyde and 100 mM of pyruvate. The optimal substrate concentration was determined with 0.1 mg mL^{-1} of *Pa*ADL^{WT} by 10−400 mM of formaldehyde or pyruvate by fixing one of both to 100 mM. Time-course reactions were made with 0.1 mg mL^{-1} of *Pa*ADL^{WT} and its variant, 100 mM of formaldehyde, and 200 mM of pyruvate.

One-Pot 2-Keto-4-hydroxybutyrate Production from Methanol. The *in vitro* enzymatic cascade reactions of *Lx*MDH^{E396V} and *Pa*ADL^{WT}, *Pa*ADL^{V121A}, *Pa*ADL^{L241A}, or *Pa*ADL$^{V121A/L241A}$ were performed with 0.5 mg mL^{-1} of *Pa*ADLs, 0.1 mg mL^{-1} of *Lx*MDH^{E396V}, 2 M of methanol, 100 mM of pyruvate, 5 mM of Mg^{2+}, and 3 mM of NAD^+ (as cofactor for *Lx*MDH^{E396V}) in 50 mM CHES buffer (pH 9.0) at 50 °C for 3 h.

HPLC Analysis. The concentration of formaldehyde, pyruvate, and 2-keto-4-hydroxybutyrate was determined by high-performance liquid chromatography (HPLC) on a Gemini 5 μm C18 110 Å, LC column 250 × 4.6 mm (Phenomenex, Torrance, CA) after derivatization with *o*-benzylhydroxylamine hydrochloride. Derivatization of samples was performed by mixing 15 μL of sample and 50 μL of 130 mM *o*-benzylhydroxylamine hydrochloride (dissolved in pyridine/methanol/water = 33:15:2) and incubation at 25 °C for 2 h. Methanol (30 μL) was added to the sample solution and then filtered through a 0.2 μm membrane filter before being injected to HPLC analysis. For quantitation, the peak areas of commercial formaldehyde, pyruvate, and 2-ketobutyric acid were used to construct the calibration curve for 2-keto-4-hydroxybutyrate.

The HPLC system (SHIMADZU, Kyoto, Japan) was composed of a SCL-40 system controller, a LC-40D solvent delivery module, a DGU-405 degassing unit, a SIL-40 autosampler, a CTO-40S column oven, and a SPD-40 UV−vis detector. Mobile phases were (A) 0.1% (v/v) of trifluoroacetic acid (TFA) in distilled water and (B) 0.095% (v/v) of TFA in ACN/distilled water = 4:1. Gradient elution was performed as follows: the concentration of B was increased from 10 to 100% from 0 to 30 min, decreased to 10% until 32 min, and finally stabilized at 10% until 50 min with 1 mL min^{-1} of flow rate. Products were detected at a wavelength of 215 nm, and the column temperature was maintained at 30 °C.

RESULTS AND DISCUSSION

Identification of *Pa*ADL. A putative aldolase from *Pa*ADL was searched by referring the sequence of *Ec*YfaU and phylogenetic analysis. *Pa*ADL has a sequential identity of

https://doi.org/10.1021/acs.jafc.2c09108
J. Agric. Food Chem. 2023, 71, 4328−4336

56.8, 64.9, and 57.2% with *Ec*YfaU, 4-hydroxy-2-ketoheptane-1,7-dioate aldolase (HpcH), and 4-hydroxy-2-oxovalerate aldolase (AkbF), respectively (Figure S1). Recombinant MBP-*Pa*ADL and *Pa*ADL had approximate molecular masses of 71.8 and 28.5 kDa, respectively, as determined by SDS-PAGE (Figure S2).

The catalytic activity of *Pa*ADL in converting formaldehyde and pyruvate to 2-keto-4-hydroxybutyrate was measured by analyzing a reaction mixture using HPLC. *Pa*ADL showed a maximum activity at 45 °C (Figure 1A) and at pH 8.5 in the EPPS buffer; however, in CHES buffer, *Pa*ADL showed higher activity at pH 9.0 than at pH 8.5 (Figure 1B). Thus, we chose pH 9.0 and CHES buffer as the optimal pH and buffer, respectively. Notably, the enzyme activity of *Ec*YfaU was tested at 25[21] or 30 °C,[28] and those of *Ec*KHB, *Rn*KHG, *Hs*KHG, and *Bt*KHG were done at pH 7.0 and 30 °C.[21,28] This suggests that the activity of *Pa*ADL may be optimized for higher temperatures than other pyruvate-converting aldolases. To compare the activity of *Pa*ADL with *Ec*YfaU, *Ec*KHB, *Rn*KHG, *Hs*KHG, and *Bt*KHG in the previous work, we calculated the enzyme activities of *Pa*ADL and *Ec*YfaU. *Ec*YfaU showed a 1.21-fold lower activity than *Ec*KHB and 12.2-, 13.4-, and 16.8-fold higher activity than *Rn*KHG, *Hs*KHG, and *Bt*KHG, respectively.[28] Moreover, the specific activity of *Pa*ADL was 5.87 nmol min^{-1} mg^{-1} (Table 1), which was 1.7-fold higher than *Ec*YfaU (3.48 nmol min^{-1} mg^{-1} in this study).

Table 1. Specific Activities of *Pa*ADL Variants[a]

enzyme	specific activity (nmol min^{-1} mg^{-1})
wild type	5.87 ± 0.04
W22A	0.67 ± 0.50
D45A	NA
R73A	NA
V121A	7.19 ± 0.11
L125A	2.34 ± 0.21
N132A	NA
P176A	NA
P189A	1.88 ± 0.13
G190A	1.96 ± 0.05
L215A	NA
S216A	1.53 ± 0.20
A217Q	1.48 ± 0.53
D218A	0.71 ± 0.34
E219A	1.37 ± 0.31
L221A	2.25 ± 0.05
V237A	6.41 ± 0.03
S240A	1.80 ± 0.30
L241A	7.34 ± 0.02
L241V	5.44 ± 0.02
L241G	3.58 ± 0.07
R244A	2.24 ± 0.70
V121A/L241A	7.54 ± 0.001

[a]NA, no activity.

Class II aldolases are divalent metal ion-dependent metalloenzymes.[40,41] *Pa*ADL showed the best catalytic efficiency in the presence of 1 mM Mg^{2+} among the metal ions tested (Figure 1C,D). The catalytic activity of *Ec*YfaU was also Co^{2+} ion-dependent,[21] which indicates a diversity of metal dependency even among aldolases that catalyze the same chemical reactions.

Structural Features of *Pa*ADL. For the structure-based enzyme engineering of *Pa*ADL, we solved its crystal structure at a resolution of 2.5 Å (Table S2). The refined single polypeptide chain of *Pa*ADL (Asp2-Lys254) shows a typical triosephosphate isomerase (TIM)-barrel fold (Figure S3).[42] Another N-terminal α-helix (α0) is found on one side of the TIM barrel, with the other side exposed to the solvent (Figure S3A).[42] The C-terminal α8-helix protrudes and interacts with two helices of α1 and α8 of a neighboring protomer (Figure S3B).

The six *Pa*ADL molecules in the asymmetric unit form a hexameric structure (Figure 2A,B) that can be subdivided into a dimer of two trimers (top trimer and bottom trimer) (Figure

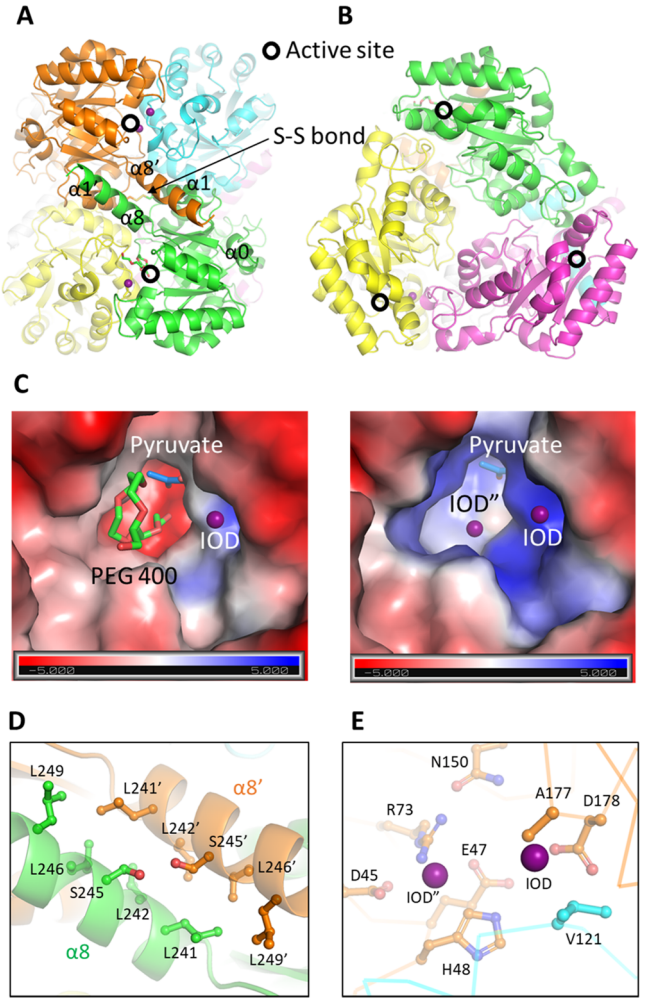

Figure 2. Crystal structure of *Pa*ADL. Side (A) and top (B) views of a cartoon diagram of the hexameric *Pa*ADL structure (PDB ID 7V8T). The six *Pa*ADL protomers in the asymmetric unit are differentiated by color. The active sites are indicated with black circles, and the disulfide (S−S) bond formed between protomers is with an arrow. (C) Surface potential mapping of the active site of *Pa*ADL. The surface potential is visualized as a color ramp from blue (positive) to red (negative). The pyruvate in *Ec*YfaU (PDB ID 2VWT) is displayed as a stick model (blue) after superposition of *Pa*ADL. The bound PEG400 and iodide ions (IOD and IOD″) are displayed with a stick model and a purple sphere, respectively. (D) Intermolecular interface: residues at the junction of the two helices are indicated with stick models. (E) A ribbon diagram of the active site of *Pa*ADL. The key residues for activity are displayed with stick models. Iodide ions (IOD and IOD″) are depicted with a purple sphere.

https://doi.org/10.1021/acs.jafc.2c09108
J. Agric. Food Chem. 2023, 71, 4328−4336

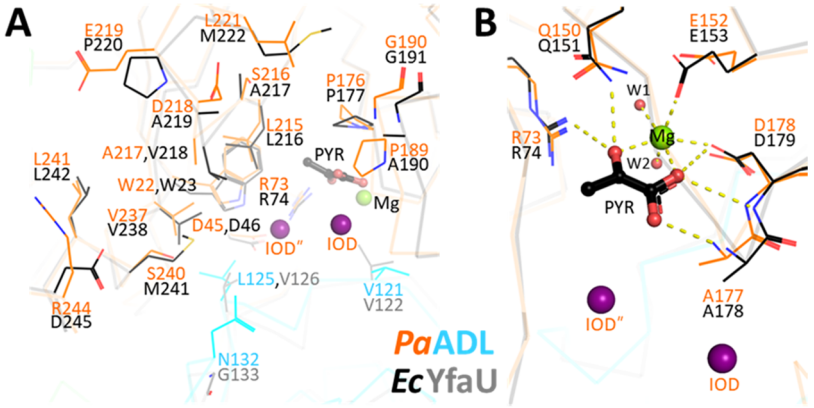

Figure 3. Superposition of the *Pa*ADL (orange and cyan) and *Ec*YfaU (blue and gray) structures. (A) Superimposition of *Pa*ADL and *Ec*YfaU in complex with pyruvate (PYR) as the substrate and selected residues for mutation are indicated by a ball-and-stick and thin stick model, respectively. (B) Zoomed-in view of the substrate binding site between *Pa*ADL and *Ec*YfaU. Two iodide ions (IOD and IOD″), one Mg^{2+} ion, and two water molecules (W1 and W2) are displayed with purple, green, and red spheres, respectively. The polar interactions between atoms are indicated with yellow-dotted lines.

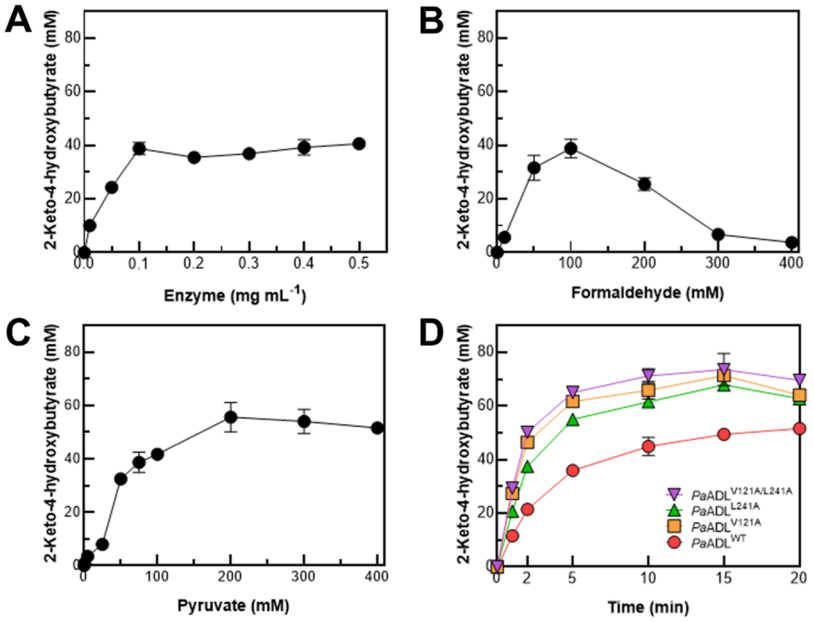

Figure 4. *Pa*ADL activity according the to enzyme and substrate concentration and reaction time. The reactions were performed in 50 mM CHES buffer (pH 9.0) with 1 mM of Mg^{2+} for 10 min at 45 °C. (A) Effect of *Pa*ADL concentration on 2-keto-4-hydroxybutyrate production from formaldehyde and pyruvate as substrates. The reaction mixture contained 100 mM of formaldehyde, 100 mM of pyruvate, and different concentrations of enzyme. (B) Effect of formaldehyde concentration on *Pa*ADL activity. The reaction mixture contained 0.1 mg mL^{-1} of crude enzyme and various concentrations of formaldehyde. (C) Effect of pyruvate concentration on *Pa*ADL activity. The reaction mixture contained 0.1 mg mL^{-1} of enzyme and various concentrations of pyruvate. (D) Comparison of activity between *Pa*ADL wild type and its variants for the production of 2-keto-4-hydroxybutyrate. The reactions were performed with 0.1 mg mL^{-1} of each enzyme, 100 mM of formaldehyde, and 200 mM of pyruvate. All experiments were performed at least twice.

2A). The bottom trimer locates three C-terminal α8-helices of each protomer upward, which form a hydrophobic interaction with residues of the downward α8- and α1-helices of the top trimer. Therefore, the dimerization of two trimers through the exchange of these α8-helices generates a hexameric assembly similar to that observed in the *Ec*YfaU structure.[41] Notably, Cys30 of the α1-helix of one protomer of the top trimer forms a disulfide bond with the same residue of another protomer of the bottom trimer (Figure 2A), thereby introducing a tight interaction between the two trimers. However, this intermolecular disulfide bridge is missing in the hexameric assembly of *Ec*YfaU.[41] Furthermore, Cys30 of *Pa*ADL is not conserved in the *Ec*YfaU (Met31), HpcH (Ser27), and AkbF (Ser30) aldolases (Figure S1), which probably provides a molecular basis for the thermostability of *Pa*ADL.

Collectively, the hexameric *Pa*ADL structure adopts typical structural features of other aldolases, except for the disulfide bond formed between the two trimers of *Pa*ADL.

Active Site. The solvent-accessible side of the TIM barrel of each protomer has a deep and wide pocket that is partly covered with an elongated region (Val111−Glu136) of a neighboring protomer in *Pa*ADL. This pocket possesses nonprotein molecules taken probably from the crystallizing reagent. One iodide ion commonly found in all six protomers

https://doi.org/10.1021/acs.jafc.2c09108
J. Agric. Food Chem. 2023, 71, 4328−4336

Table 2. Kinetic Parameters of *Ec*YfaU and *Pa*ADL Variants with Formaldehyde and Pyruvate[a,b]

	formaldehyde			pyruvate			
enzyme	k_{cat} (min^{-1})	K_m (mM)	k_{cat}/K_m (min^{-1} mM^{-1})	k_{cat} (min^{-1})	K_m (mM)	k_{cat}/K_m (min^{-1} mM^{-1})	ref
*Ec*YfaU	113 ± 40	24 ± 4	4.71	113 ± 40	209 ± 83	0.54	32
*Pa*ADL^{WT}	271 ± 13	45 ± 5.4	6.02 ± 0.8	255 ± 11	37 ± 4.4	6.8 ± 0.9	in this study
*Pa*ADL^{V121A}	348 ± 17	35 ± 4.9	10 ± 1.5	393 ± 12	41 ± 3.1	9.5 ± 0.7	
*Pa*ADL^{L241A}	432 ± 19	65 ± 5.9	6.6 ± 0.7	421 ± 23	68 ± 7.8	6.2 ± 0.8	
*Pa*ADL$^{V121A/L241A}$	398 ± 18	35 ± 4.4	11 ± 1.5	453 ± 15	52 ± 3.8	8.8 ± 0.7	

[a]Steady-state kinetic parameters were determined using a fit of the Michaelis−Menten equation to the initial velocity as a function of substrate concentration. [b]The reaction involving *Pa*ADL was performed in 50 mM CHES buffer (pH 9.0) containing 1 mM of Mg^{2+} at 45 °C for 10 min.

occupies a space formed by residues of Ala177 and Phe189 (Figures 2C and S4D). The other iodide ion is located in the space formed by Leu215 and Ala177 of one protomer and Ala124 of another protomer (Figure 2D) and is far from the first iodide ion by ∼6 Å (Figure 2D). The second iodide is replaced with an elongated electron density that was tentatively modeled as PEG400 in the two protomers. One of its terminal oxygen atoms is located in the polar environment formed by the side chains of Arg73 and Asp178 of one molecule and the carbonyl oxygen of Val121 of the neighboring molecule (Figures 2E and S3E). Interestingly, two PEG-containing protomers are found at each trimer.

The crystal structure of *Ec*YfaU pyruvate aldolase in complex with pyruvate has been revealed[41] and can be superposed on the crystal structure of *Pa*ADL pyruvate aldolase. Critical residues in the substrate binding site are also conserved between *Ec*YfaU and *Pa*ADL spatially, indicating that the sequence and structural comparison of the pyruvate binding site in *Pa*ADL are reasonable (Figure 3). The sequence and structural comparison of *Pa*ADL with other related enzymes indicate the presence of several conserved residues; for example, Asp45 and Arg73, within this pocket (Figures 3A and S1). Mutation of these residues abolished the catalytic activity of *Pa*ADL (Figures S4 and S5), indicating that they are indispensable for the aldolase activity of *Pa*ADL. Because residues interacting with the Mg^{2+} ion and pyruvate are highly conserved (Figures 4B and S1), it is highly plausible that *Pa*ADL may share a common enzymatic mechanism with other related enzymes.[41,43]

Molecular Characterization of *Pa*ADL and Its Variants. Residues at the entrance of the active site affect the catalytic activity of the enzyme by regulating the transport of substrates into and products from the active site.[44] Also, the subunit interface is related with the catalytic activity of oligomeric proteins.[45]

To identify residues affecting the catalytic activity of *Pa*ADL, its structure was superimposed on the pyruvate-bound *Ec*YfaU (Figure 3A). Then, we introduced alanine-scanning mutations into residues in the active site, including the entrance of the active site and at the protomer−protomer interfaces (Figure S3), and their activities were compared with respect to the wild-type enzyme (Figures S4−S6). As expected, mutations around the expected pyruvate binding sites (N132A, P176A, and L215A) of *Pa*ADL depleted the aldolase activity. On the other hand, the replacement of Val121 and Leu241 with the respective alanine residues (*Pa*ADL^{V121A} and *Pa*ADL^{L241A}) increased the aldol condensation activity by 1.22- and 1.25-folds, compared with the wild-type enzyme, respectively (Table 1). Remarkably, these two residues are located far from the active site and are commonly located at the interface of neighboring protomers (Figure 3A). As mentioned above, Val121 at the elongated region (Val111−Glu136) partly covers the active site of the neighboring protomer and Leu241 on the protruding α8-helix hydrophobically interacts with Leu241 on the α8-helix of the neighboring protomer. Further mutations of Leu241 with valine or glycine decreased its respective catalytic activity, suggesting the importance of its side chain length here. A double mutation at these two residues (*Pa*ADL$^{V121A/L241A}$) showed a catalytic activity slightly higher than that of *Pa*ADL^{V121A} or *Pa*ADL^{L241A} (Table 1), indicating that their synergistic effect is not as high as expected. According to the structure, these two residues are located far from the active site and separated from each other. For this reason, a double mutant may show very low synergic effect. In the future, other protein engineering strategies, such as error-prone PCR, DNA shuffling with other pyruvate aldolases, or deep-learning studies, could be considered for the improvement of *Pa*ADL or the activities of other enzymes.

Kinetics of *Pa*ADL and Its Variants. The kinetic parameters of *Pa*ADLs were determined using formaldehyde and pyruvate as substrates (Table 2). The activities of *Pa*ADL and its variant enzymes increased with the concentration of formaldehyde or pyruvate up to 100 mM and maintained similar values up to 150 mM of substrates. Therefore, kinetic parameters were estimated at formaldehyde or pyruvate concentrations below 150 mM (Figure S7).

The k_{cat}, K_m, and k_{cat}/K_m of *Pa*ADL^{WT} toward formaldehyde exhibited 2.4-, 1.9-, and 1.3-folds, respectively, higher values than those of *Ec*YfaU (Table 2).[32] Conversely, the k_{cat} and k_{cat}/K_m values of *Pa*ADL^{WT} toward pyruvate were 255 min^{-1} and 6.8 min^{-1} mM^{-1}, which are 2.3- and 12.6-folds higher, respectively, than those of *Ec*YfaU (Table 2). Additionally, to compare substrate tolerance, we measured the activity of *Ec*YfaU at different substrate concentrations (Figure S7). *Ec*YfaU seems to be inhibited at concentrations above 80 mM of formaldehyde and 40 mM of pyruvate, which is consistent with previous work by Bosch et al.[32] These results suggest that the *Pa*ADL-catalyzed condensation of formaldehyde with pyruvate to produce 2-keto-4-hydroxybutyrate is more efficient than that catalyzed by *Ec*YfaU.

The K_m values of *Pa*ADL^{WT} toward formaldehyde and pyruvate are 45 and 37 mM, respectively. Compared with *Pa*ADL^{WT}, the *Pa*ADL^{V121A} variant showed similar or lower K_m values toward formaldehyde (35 mM) and pyruvate (41 mM) and, thus, higher catalytic efficiency. However, the *Pa*ADL^{L241A} variant showed significantly increased K_m values for formaldehyde (65 mM) and pyruvate (68 mM) and 1.59 and 1.65-fold higher k_{cat} values, respectively, than *Pa*ADL^{WT}, indicating that its k_{cat}/K_m values were similar to those of *Pa*ADL^{WT}. To overcome the increased K_m values of *Pa*ADL^{L241A}, we constructed a double variant (*Pa*ADL$^{V121A/L241A}$). The k_{cat} values of *Pa*ADL$^{V121A/L241A}$ for the two substrates were

https://doi.org/10.1021/acs.jafc.2c09108
J. Agric. Food Chem. 2023, 71, 4328−4336

maintained, but K_m values were not significantly changed, so its variant showed a slight synergistic effect even though *Pa*ADL$^{V121A/L241A}$ exhibited 1.8- and 1.3-fold higher k_{cat}/K_m values than *Pa*ADL^{WT}. Moreover, *Pa*ADL^{V121A} showed the highest k_{cat}/K_m values among the *Pa*ADL variants, but this result is not consistent with specific activity; it seemed to be affected by the difference of enzyme and substrate concentrations. Thus, we conducted the next experiments, such as 2-keto-4-hydroxybutyrate production, to compare the amount of product, productivities, and specific productivities between *Pa*ADL^{WT} and variant enzymes.

Bioconversion of 2-Keto-4-hydroxybutyrate from Formaldehyde and Pyruvate. To investigate the optimal enzyme concentration for the 2-keto-4-hydroxybutyrate production, 0.01−0.5 mg mL^{-1} of *Pa*ADL^{WT} was incubated with 100 mM of formaldehyde and 100 mM of pyruvate in the presence of 1 mM of Mg^{2+}. The product increased with a maximum value of 40.6 mM when less than 0.1 mg mL^{-1} of enzyme was used but reached a plateau with above 0.1 mg mL^{-1} of enzyme (Figure 4A). Next, we determined the optimal substrate concentrations for the reaction. When 0−400 mM of formaldehyde or pyruvate was tested with 0.1 mg mL^{-1} of enzyme, the maximal production of 2-keto-4-hydroxybutyrate occurred at substrate concentrations of 100 mM of formaldehyde and 200 mM of pyruvate (Figure 4B,C).

Under these optimized reaction conditions, the time-course reactions were conducted for the production of 2-keto-4-hydroxybutyrate using *Pa*ADL^{WT}, *Pa*ADL^{V121A}, *Pa*ADL^{L241A}, and *Pa*ADL$^{V121A/L241A}$ (Figure 4D). *Pa*ADL^{WT} produced 51.6 mM (6.03 g L^{-1}) of 2-keto-4-hydroxybutyrate from 100 mM of formaldehyde and 200 mM of pyruvate for 15 min, corresponding to a productivity of 24.2 g L^{-1} h^{-1} (Figure 4D). On the other hand, the produced amount of 2-keto-4-hydroxybutyrate by *Pa*ADL^{V121A}, *Pa*ADL^{L241A}, and *Pa*ADL$^{V121A/L241A}$ reached 71.3 mM (8.33 g L^{-1}), 67.9 mM (7.94 g L^{-1}), and 73.6 mM (8.60 g L^{-1}), respectively. These values correspond to 33.4, 31.8, and 34.5 g L^{-1} h^{-1}, which were 1.38-, 1.31-, and 1.42-fold higher than *Pa*ADL^{WT}, respectively. Furthermore, the specific productivities of *Pa*ADL^{WT}, *Pa*ADL^{V121A}, *Pa*ADL^{L241}, and *Pa*ADL$^{V121A/L241A}$ were 234.5, 334.0, 317.9, and 334.6 mg mg-enzyme^{-1} h^{-1}, respectively. In the presence of high concentrations of enzymes and substrates, *Pa*ADL$^{V121A/L241A}$ exhibited slightly higher specific productivity than other enzymes. To the best of our knowledge, this is the first enzyme-based report for the high production of 2-keto-4-hydroxybutyrate as the main product using optimized conditions of each substrate and enzyme.

One-Pot Biosynthesis of 2-Keto-4-hydroxybutyrate from Methanol and Pyruvate Using *Lx*MDH and *Pa*ADL. The worldwide methanol production capacity reached 110 million metric tons in 2018.[1] *Lx*MDH is a redox enzyme that mediates the reversible bioconversion of methanol to formaldehyde, and its variants (*Lx*MDH^{K318N} and *Lx*MDH^{E396V}) have shown much increased affinity for methanol than the wild-type enzyme in the presence of 5 mM of Mg^{2+} and 3 mM of NAD^+.[13,14] Therefore, we explored a one-pot reaction for the biosynthesis of 2-keto-4-hydroxybutyrate from methanol as a C1 chemical and pyruvate using *Lx*MDH and *Pa*ADL to take advantages of synergistic simultaneous processing by the enzyme cascade reaction.[46,47]

*Lx*MDH^{K318N} and *Lx*MDH^{E396V} produced 0.07 and 0.1 mM of formaldehyde from 2 M methanol for 30 min, respectively (Figure S8A), suggesting that the latter is a better candidate for the cascade reaction with *Pa*ADL. Notably, formaldehyde produced by these two variants decreased within 2 h, probably due to preference of the enzymes for the reduction reaction, i.e., formaldehyde to methanol.

Next, we investigated the optimal concentration of enzymes and substrates (Figure S8B,C). The combination of 0.1 mg mL^{-1} of *Lx*MDH^{E396V} and 0.5 mg mL^{-1} of *Pa*ADL^{WT} yielded 0.4 mM of 2-keto-4-hydroxybutyrate at pH 9.0 and 50 °C from 2 M of methanol, 5 mM of pyruvate, 5 mM of Mg^{2+}, and 3 mM of NAD^+ after 4 h. To investigated the effect of the Mg^{2+} concentration in the cascade reaction, the reactions were performed with Mg^{2+} varying from 1 to 10 mM, which showed that the Mg^{2+} concentration was not critical for the reaction (Figure S8D). Nevertheless, MDH activity as the first step is quite critical as the supplement of formaldehyde for 2-keto-4-hydroxybutyrate production. Thus, we performed the cascade reaction at 5 mM of Mg^{2+} for the enzymatic activity of *Lx*MDH. Moreover, there was limitation to producing formaldehyde from methanol using *Lx*MDH because this enzyme can produce approximately 1 mM of formaldehyde. Thus, we investigated the one-pot production of 2-keto-4-hydroxybutyrate from 2 M methanol and 100 mM pyruvate with 5 mM of Mg^{2+} and 3 mM of NAD^+ by 0.1 mg mL^{-1} of *Lx*MDH^{E396V} and 0.5 mg mL^{-1} of *Pa*ADL$^{V121A/L241A}$ (Figure 5). Under these reaction conditions, *Lx*MDH^{E396V} and

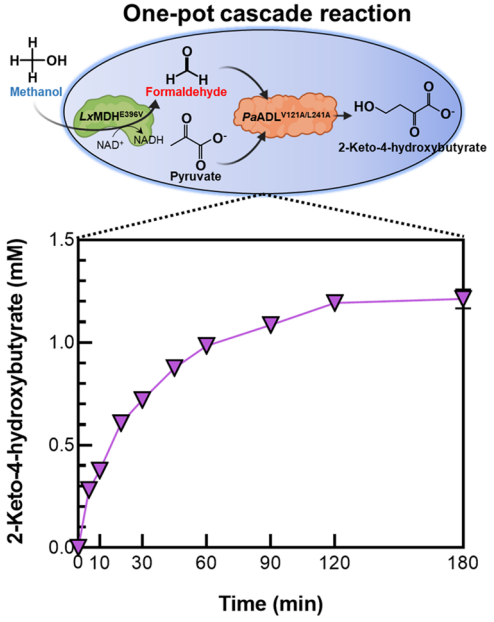

Figure 5. One-pot cascade reaction using *Lx*MDH^{E396V} and *Pa*ADL$^{V121A/L241A}$ for the production of 2-keto-4-hydroxybutyrate from methanol and pyruvate. The reactions were performed in 50 mM CHES buffer (pH 9.0) with 0.1 mg mL^{-1} of *Lx*MDH^{E396V} and 0.5 mg mL^{-1} of *Pa*ADL$^{V121A/L241A}$, 3 mM of NAD^+, 5 mM of Mg^{2+}, 2 M of methanol, and 100 mM of pyruvate. All experiments were performed at least twice.

*Pa*ADL$^{V121A/L241A}$ yielded 1.22 mM (142.7 mg L^{-1}) of 2-keto-4-hydroxybutyrate for 2 h, corresponding to a productivity of 71.4 mg L h^{-1}. It is worthwhile mentioning that this is the first challenge of a C4 chemical production with methanol as a C1 chemical by the one-pot cascade system *in vitro*, suggesting that an enzyme cascade reaction of *Lx*MDH and *Pa*ADL is an economical and meaningful process for the production of multicarbon chemicals from C 1s.

https://doi.org/10.1021/acs.jafc.2c09108
J. Agric. Food Chem. 2023, 71, 4328−4336

In conclusion, the development of the C1 compound-utilizing and -assimilating pathway is becoming an important area for producing value-added products. We characterized a new pyruvate aldolase *Pa*ADL and engineered it to possess higher activity toward formaldehyde and pyruvate than other known aldolases. We further constructed a cascade reaction, using *Lx*MDH and *Pa*ADL, to allow a net incorporation of methanol into pyruvate to produce 2-keto-4-hydroxybutyrate. There are still some bottlenecks that should be overcome, for example, thermostability and further enhancement of the catalytic activity of MDH, and regeneration of cofactor produced during the cascade reaction. Nonetheless, to the best of our knowledge, this is the first study to perform the quantitative biocatalytic synthesis of 2-keto-4-hydroxybutyrate as the main product from methanol via an enzymatic reaction. Our results will contribute to the industrial application of pyruvate aldolase-based biocatalysts for the production of high-value compounds from inexpensive C1 chemicals using green and eco-friendly processes.

■ ASSOCIATED CONTENT

Supporting Information

The Supporting Information is available free of charge at https://pubs.acs.org/doi/10.1021/acs.jafc.2c09108.

Strains, plasmids, and oligonucleotides used in this study (Table S1); data collection and refinement statistics (Table S2); phylogenetic tree and sequence alignment of *Pa*ADL and other class II pyruvate aldolases (Figure S1); SDS-PAGE analysis of recombinant *Pa*ADL (Figure S2); crystal structure of *Pa*ADL (Figure S3); comparison of *Pa*ADL activities with wild type and its variants (Figure S4); SDS-PAGE analysis of *Pa*ADL variants (Figure S5); HPLC chromatogram for the reaction of *Pa*ADL variants (Figure S6); kinetic parameters of aldol condensation of formaldehyde and pyruvate catalyzed by $PaADL^{WT}$, $PaADL^{V121A}$, $PaADL^{L241A}$, and $PaADL^{V121A/L241A}$ (Figure S7); and synthesis of 2-keto-4-hydroxybutyrate from methanol and pyruvate and relative references (Figure S8) (PDF)

■ AUTHOR INFORMATION

Corresponding Authors

Jeong-Sun Kim − *Department of Chemistry, Chonnam National University, Gwangju 61186, Republic of Korea*; Phone: +82-62-530-3384; Email: jsunkim@chonnam.ac.kr

Soo-Jin Yeom − *School of Biological Sciences and Biotechnology, Graduate School, Chonnam National University, Gwangju 61186, Republic of Korea; School of Biological Sciences and Technology, Chonnam National University, Gwangju 61186, Republic of Korea*; orcid.org/0000-0001-7307-237X; Phone: +82-62-530-1911; Email: soojin258@jnu.ac.kr

Authors

Yeon-Ju Jeong − *School of Biological Sciences and Biotechnology, Graduate School, Chonnam National University, Gwangju 61186, Republic of Korea*

Pil-Won Seo − *Department of Chemistry, Chonnam National University, Gwangju 61186, Republic of Korea*

Min-Ju Seo − *School of Biological Sciences and Technology, Chonnam National University, Gwangju 61186, Republic of Korea*

Su-Bin Ju − *School of Biological Sciences and Biotechnology, Graduate School, Chonnam National University, Gwangju 61186, Republic of Korea*

Complete contact information is available at: https://pubs.acs.org/10.1021/acs.jafc.2c09108

Author Contributions

‖Y.-J. J., P.-W.S., and M.-J.S. contributed equally to this work. The manuscript was written through contributions of all authors. All authors have given approval to the final version of the manuscript.

Funding

This work was supported by grants from the C1 Gas Refinery Program, funded by the Ministry of Science and ICT (NRF-2018M3D3A1A01056181 and 2018M3D3A1A01055735).

Notes

The authors declare no competing financial interest.

■ ACKNOWLEDGMENTS

The X-ray diffraction experiments were performed using Beamline 11C at the Pohang Accelerator in Korea.

■ REFERENCES

(1) Jiang, W.; Hernandez Villamor, D.; Peng, H.; Chen, J.; Liu, L.; Haritos, V.; Ledesma-Amaro, R. Metabolic engineering strategies to enable microbial utilization of C1 feedstocks. *Nat. Chem. Biol.* **2021**, *17*, 845−855.

(2) Narine, K.; Mahabir, J.; Koylass, N.; Samaroo, N.; Singh-Gryzbon, S.; Baboolal, A.; Guo, M.; Ward, K. Climate smart process design for current and future methanol production. *J. Co2 Util.* **2021**, *44*, 44.

(3) He, H.; Hoper, R.; Dodenhoft, M.; Marliere, P.; Bar-Even, A. An optimized methanol assimilation pathway relying on promiscuous formaldehyde-condensing aldolases in *E. coli*. *Metab. Eng.* **2020**, *60*, 1−13.

(4) Meyer, F.; Keller, P.; Hartl, J.; Groninger, O. G.; Kiefer, P.; Vorholt, J. A. Methanol-essential growth of *Escherichia coli*. *Nat. Commun.* **2018**, *9*, No. 1508.

(5) Chen, F.-H.; Jung, H. W.; Tsuei, C. Y.; Liao, J. C. Converting *Escherichia coli* to a Synthetic Methylotroph Growing Solely on Methanol. *Cell* **2020**, *182*, 933−946.

(6) Jo, H. J.; Kim, J. H.; Kim, Y. N.; Seo, P. W.; Kim, C. Y.; Kim, J. W.; Yu, H. N.; Cheon, H.; Lee, E. Y.; Kim, J. S.; Park, J. B. Glyoxylate carboligase-based whole-cell biotransformation of formaldehyde into ethylene glycol via glycotaldehyde. *Green. Chem.* **2022**, *24*, 218−226.

(7) Desmons, S.; Fauré, R.; Bontemps, S. Formaldehyde as a promising C1 source: the instrumental role of biocatalysis for stereocontrolled reactions. *ACS Catal.* **2019**, *9*, 9575−9588.

(8) Schrader, J.; Schilling, M.; Holtmann, D.; Sell, D.; Filho, M. V.; Marx, A.; Vorholt, J. A. Methanol-based industrial biotechnology: current status and future perspectives of methylotrophic bacteria. *Trends Biotechnol.* **2009**, *27*, 107−115.

(9) Du, X. L.; Jiang, Z.; Su, D. S.; Wang, J. Q. Research Progress on the Indirect Hydrogenation of Carbon Dioxide to Methanol. *ChemSusChem* **2016**, *9*, 322−332.

(10) Wang, Y.; Fan, L.; Tuyishime, P.; Zheng, P.; Sun, J. Synthetic Methylotrophy: A Practical Solution for Methanol-Based Biomanufacturing. *Trends Biotechnol.* **2020**, *38*, 650−666.

(11) Le, T.-K.; Lee, Y.-J.; Han, G. H.; Yeom, S.-J. Methanol dehydrogenases as a key biocatalysts for synthetic methylotrophy. *Front. Bioeng. Biotech.* **2021**, *9*, 1345.

(12) Woolston, B. M.; King, J. R.; Reiter, M.; Van Hove, B.; Stephanopoulos, G. Improving formaldehyde consumption drives methanol assimilation in engineered *E. coli*. *Nat. Commun.* **2018**, *9*, No. 2387.

(13) Lee, J. Y.; Park, S. H.; Oh, S. H.; Lee, J. J.; Kwon, K. K.; Kim, S. J.; Choi, M.; Rha, E.; Lee, H.; Lee, D. H.; Sung, B. H.; Yeom, S. J.; Lee, S. G. Discovery and Biochemical Characterization of a Methanol Dehydrogenase From *Lysinibacillus xylanilyticus*. *Front. Bioeng. Biotech.* **2020**, *8*, 67.
(14) Le, T. K.; Ju, S. B.; Lee, H. W.; Lee, J. Y.; Oh, S. H.; Kwon, K. K.; Sung, B. H.; Lee, S. G.; Yeom, S. J. Biosensor-Based Directed Evolution of Methanol Dehydrogenase from *Lysinibacillus xylanilyticus*. *Int. J. Mol. Sci.* **2021**, *22*, 1471.
(15) Robins, K.; Osorio-Lozada, A.; Avi, M.; Richter, M. 7.23 New Emerging Reactions. In *Comprehensive Chirality*, 2012; pp 481−515.
(16) Zheng, W. L.; Chen, K. T.; Wang, Z.; Cheng, X. L.; Xu, G.; Yang, L. R.; Wu, J. P. Construction of a Highly Diastereoselective Aldol Reaction System with L-Threonine Aldolase by Computer-Assisted Rational Molecular Modification and Medium Engineering. *Org. Lett.* **2020**, *22*, 5763−5767.
(17) Walters, M. J.; Toone, E. J. Pyruvate aldolases in chiral carbon-carbon bond formation. *Nat. Protoc.* **2007**, *2*, 1825−1830.
(18) Baker, P.; Seah, S. Y. Rational design of stereoselectivity in the class II pyruvate aldolase BphI. *J. Am. Chem. Soc.* **2012**, *134*, 507−513.
(19) Hernández, K.; Joglar, J.; Bujons, J.; Parella, T.; Clapes, P. Nucleophile Promiscuity of Engineered Class II Pyruvate Aldolase YfaU from *E. coli*. *Angew. Chem. Int. Ed.* **2018**, *57*, 3583−3587.
(20) Windle, C. L.; Muller, M.; Nelson, A.; Berry, A. Engineering aldolases as biocatalysts. *Curr. Opin. Chem. Biol.* **2014**, *19*, 25−33.
(21) Hernandez, K.; Bujons, J.; Joglar, J.; Charnock, S. J.; de Maria, P. D.; Fessner, W. D.; Clapes, P. Combining Aldolases and Transaminases for the Synthesis of 2-Amino-4-hydroxybutanoic Acid. *ACS Catal* **2017**, *7*, 1707−1711.
(22) Chen, Z.; Geng, F.; Zeng, A. P. Protein design and engineering of a de novo pathway for microbial production of 1,3-propanediol from glucose. *Biotechnol. J.* **2015**, *10*, 284−289.
(23) Bouzon, M.; Perret, A.; Loreau, O.; Delmas, V.; Perchat, N.; Weissenbach, J.; Taran, F.; Marliere, P. A Synthetic Alternative to Canonical One-Carbon Metabolism. *ACS Synth. Biol.* **2017**, *6*, 1520−1533.
(24) Frazão, C. J.; Topham, C. M.; Malbert, Y.; Francois, J. M.; Walther, T. Rational engineering of a malate dehydrogenase for microbial production of 2,4-dihydroxybutyric acid via homoserine pathway. *Biochem. J.* **2018**, *475*, 3887−3901.
(25) Zhong, W. Q.; Zhang, Y.; Wu, W. J.; Liu, D. H.; Chen, Z. Metabolic Engineering of a Homoserine-Derived Non-Natural Pathway for the De Novo Production of 1,3-Propanediol from Glucose. *ACS Synth. Biol.* **2019**, *8*, 587−595.
(26) Zhang, Y.; Ma, C.; Dischert, W.; Soucaille, P.; Zeng, A. P. Engineering of Phosphoserine Aminotransferase Increases the Conversion of L-Homoserine to 4-Hydroxy-2-ketobutyrate in a Glycerol-Independent Pathway of 1,3-Propanediol Production from Glucose. *Biotechnol. J.* **2019**, *14*, No. 1900003.
(27) Frazão, C. J. R.; Trichez, D.; Serrano-Bataille, H.; Dagkesamanskaia, A.; Topham, C. M.; Walther, T.; Francois, J. M. Construction of a synthetic pathway for the production of 1,3-propanediol from glucose. *Sci. Rep.* **2019**, *9*, No. 11576.
(28) Wang, C.; Ren, J.; Zhou, L. B.; Li, Z. D.; Chen, L.; Zeng, A. P. An Aldolase-Catalyzed New Metabolic Pathway for the Assimilation of Formaldehyde and Methanol To Synthesize 2-Keto-4-hydroxybutyrate and 1,3-Propanediol in *Escherichia coli*. *ACS Synth. Biol.* **2019**, *8*, 2483−2493.
(29) Česnik, M.; Sudar, M.; Hernandez, K.; Charnock, S.; Vasic-Racki, D.; Clapes, P.; Blazevic, F. Z. Cascade enzymatic synthesis of L-homoserine - mathematical modelling as a tool for process optimisation and design. *React. Chem. Eng.* **2020**, *5*, 747−759.
(30) Xu, Y. Y.; Meng, H.; Ren, J.; Zeng, A. P. Formaldehyde formation in the glycine cleavage system and its use for an aldolase-based biosynthesis of 1,3-propanediol. *J. Biol. Eng.* **2020**, *14*, 15.
(31) Česnik, M.; Sudar, M.; Hernandez, K.; Qi, Y. Y.; Charnock, S. J.; Vasic-Racki, D.; Clapes, P.; Blazevic, Z. F. Cascade Synthesis of L-Homoserine Catalyzed by Lyophilized Whole Cells Containing Transaminase and Aldolase Activities: The Mathematical Modeling Approach. *Ind. Eng. Chem. Res.* **2021**, *60*, 13846−13858.
(32) Bosch, S.; Sanchez-Freire, E.; Del Pozo, M. L.; Česnik, M.; Quesada, J.; Mate, D. M.; Hernández, K.; Qi, Y.; Clapés, P.; Vasić-Rački, Đ.; et al. Thermostability engineering of a class II pyruvate aldolase from *Escherichia coli* by in vivo folding interference. *ACS Sustainable Chem. Eng.* **2021**, *9*, 5430−5436.
(33) Aslanidis, C.; de Jong, P. J. Ligation-independent cloning of PCR products (LIC-PCR). *Nucleic Acids Res.* **1990**, *18*, 6069−6074.
(34) Xu, Q. S.; Shin, D. H.; Pufan, R.; Yokota, H.; Kim, R.; Kim, S. H. Crystal structure of a phosphotransacetylase from *Streptococcus pyogenes*. *Proteins* **2004**, *55*, 479−481.
(35) Ho, S. N.; Hunt, H. D.; Horton, R. M.; Pullen, J. K.; Pease, L. R. Site-directed mutagenesis by overlap extension using the polymerase chain reaction. *Gene* **1989**, *77*, 51−59.
(36) Larkin, M. A.; Blackshields, G.; Brown, N. P.; Chenna, R.; McGettigan, P. A.; McWilliam, H.; Valentin, F.; Wallace, I. M.; Wilm, A.; Lopez, R.; Thompson, J. D.; Gibson, T. J.; Higgins, D. G. Clustal W and Clustal X version 2.0. *Bioinformatics* **2007**, *23*, 2947−2948.
(37) Otwinowski, Z.; Minor, W. Processing of X-ray Diffraction Data Collected in Oscillation Mode. In *Methods in Enzymology*, 1997; Vol. *276*, pp 307−326.
(38) Adams, P. D.; Afonine, P. V.; Bunkoczi, G.; Chen, V. B.; Davis, I. W.; Echols, N.; Headd, J. J.; Hung, L. W.; Kapral, G. J.; Grosse-Kunstleve, R. W.; McCoy, A. J.; Moriarty, N. W.; Oeffner, R.; Read, R. J.; Richardson, D. C.; Richardson, J. S.; Terwilliger, T. C.; Zwart, P. H. PHENIX: a comprehensive Python-based system for macromolecular structure solution. *Acta. Crystallogr. D Biol. Crystallogr* **2010**, *66*, 213−221.
(39) Emsley, P.; Cowtan, K. Coot: model-building tools for molecular graphics. *Acta. Crystallogr. D Biol. Crystallogr.* **2004**, *60*, 2126−2132.
(40) Hixon, M.; Sinerius, G.; Schneider, A.; Walter, C.; Fessner, W. D.; Schloss, J. V. Quo vadis photorespiration: A tale of two aldolases. *FEBS Lett.* **1996**, *392*, 281−284.
(41) Rea, D.; Hovington, R.; Rakus, J. F.; Gerlt, J. A.; Fulop, V.; Bugg, T. D. H.; Roper, D. I. Crystal structure and functional assignment of YfaU, a metal ion dependent class II aldolase from *Escherichia coli* K12. *Biochemistry* **2008**, *47*, 9955−9965.
(42) Wierenga, R. K. The TIM-barrel fold: a versatile framework for efficient enzymes. *FEBS Lett.* **2001**, *492*, 193−198.
(43) Coincon, M.; Wang, W.; Sygusch, J.; Seah, S. Y. Crystal structure of reaction intermediates in pyruvate class II aldolase: substrate cleavage, enolate stabilization, and substrate specificity. *J. Biol. Chem.* **2012**, *287*, 36208−36221.
(44) Kokkonen, P.; Bednar, D.; Pinto, G.; Prokop, Z.; Damborsky, J. Engineering enzyme access tunnels. *Biotechnol. Adv.* **2019**, *37*, No. 107386.
(45) Malay, A. D.; Allen, K. N.; Tolan, D. R. Structure of the Thermolabile Mutant Aldolase B, A149P: Molecular Basis of Hereditary Fructose Intolerance. *J. Mol. Biol.* **2005**, *347*, 135−144.
(46) Ricca, E.; Brucher, B.; Schrittwieser, J. H. Multi-Enzymatic Cascade Reactions: Overview and Perspectives. *Adv. Synth. Catal.* **2011**, *353*, 2239−2262.
(47) Camps Bres, F.; Guerard-Helaine, C.; Helaine, V.; Fernandes, C.; Sanchez-Moreno, I.; Traikia, M.; Garcia-Junceda, E.; Lemaire, M. L-Rhamnulose-1-phosphate and L-fuculose-1-phosphate aldolase mediated multi-enzyme cascade systems for nitrocyclitol synthesis. *J. Mol. Catal. B: Enzym.* **2015**, *114*, 50−57.

https://doi.org/10.1021/acs.jafc.2c09108
J. Agric. Food Chem. 2023, 71, 4328−4336